



Experimental investigation of coatings efficiency in micro-ball-end milling of pre-sintered 5Y-TZP ceramic

Franck Marques¹ · Michaël Fontaine¹ · Alexandre Gilbin¹ · Bérenger Escolle¹ · Philippe Picart¹

Received: 5 December 2022 / Accepted: 8 December 2023 / Published online: 22 February 2024
© The Author(s), under exclusive licence to Springer-Verlag London Ltd., part of Springer Nature 2024

Abstract

This study deals with micro-ball-end milling of a pre-sintered yttria tetragonal zirconia polycrystal. The aim is to underline the reliability of different coatings while machining this material regularly used in dental and luxury industries. Micro-ball-end mills are often used to machine partially sintered ceramics in dry conditions. This process is identified as critical by tool manufacturers and users in terms of wear and machining accuracy. The purpose is then to analyse the capacity of different tool/coating couples to ensure stable micro-machining of such ceramics. Cutting forces, tool reliability and surface integrity data are obtained from green machining tests of a 5Y-TZP (tetragonal zirconia polycrystal stabilised by 5% mol of yttrium) with 1-mm-diameter tungsten carbide micro-tools coated with two PVD coatings and one CVD coating (respectively AlCrN, DLC and diamond). The results highlight that the choice of an appropriate coating is mandatory for this type of abrasive ceramics, even if they are partially sintered. Material flow, tool wear and machined surface quality are discussed and correlated.

Keywords Micro-milling · Ball-end milling · Pre-sintered ceramic Y-TZP · Green machining · Tool wear · Tool coating

1 Introduction

The increasing demand for micro-components leads to an improvement of control and development for dedicated methods in the concerned manufacturing fields. Regarding the other processes, micro-milling seems to be one of the most versatile. From a down-scaling approach of conventional machining, the term “micro-milling” is used when the concerned tools are equal or inferior to 1 mm in diameter as mentioned by Masusawa et al. [1]. This process is applicable to a wide range of materials and allows to produce three-dimensional complex geometry with relatively high shape ratio parts as presented in Friedrich et al. work (until details presenting a few tens of microns in thickness) [2]. Nonetheless, by decreasing the scale, some phenomena—generally neglected in macro-scale machining—see their impacts increase. The material removal rate is very low in front of

classical machining applications as detailed by Keong et al. for aluminium cutting [3]. On this scale, unlike macro-machining, the cutting-edge radius of the tool becomes significant enough compared to uncut chip thickness. In this context, new mechanisms of cutting that affect tool performance and surface integrity are involved, respectively, described by Aramcharoen et al. [4] and Câmara et al. [5]. Pre-sintered ceramics have particular mechanical behaviour in front of metallic materials. Mohanty et al. [6] underlined the brittle behaviour of green alumina, and Dadhich et al. [7] investigated an alternative way to machine these materials by confronting contact versus non-contact machining. Besides, it has been proved that depending on the tool coating/machined material couple, tool wear is different and can even break the mill as proved by Uçun et al. [8]. Researches by De Cristofaro et al. underline the importance of having a net-shaped coating in particular abrasive conditions [9].

In their review article published in 2022 and based on 43 reference papers, Herràez-Galindo et al. [10] precise that zirconium has favourable mechanical properties as well as high biological stability and biocompatibility, and its surface has low plaque retention for dental applications. Its relative opacity can be corrected when stabilised with yttrium and can potentially avoid the use of feldspathic ceramics at upper

✉ Michaël Fontaine
michael.fontaine@ens2m.fr

¹ Université de Franche-Comté, SUPMICROTECH, CNRS, FEMTO-ST Institute, Applied Mechanics Dept., 24 rue de L'épitahe, F-25000 Besançon, France

surface. This material also exhibits favourable mechanical properties, largely due to the particle size in the structure (0.2–0.5 μm), which helps maintain the stable tetragonal phase. It presents high flexural strength (900–1200 MPa), fracture resistance (7–10 $\text{MPa}\cdot\text{m}^{1/2}$) and elasticity modulus (210 GPa) [10]. Like metals, zirconia can be presented in different solid phases: monoclinic, tetragonal and cubic. Sintering at close to 2000 °C for several hours enables the transition from a monoclinic to a tetragonal phase. Sintering pure zirconia can create cracks or even cause the part to burst in extreme cases during the cooling phase [11]. Nevertheless, this property is used to slow the progression of cracks within a part, but the material used contains an element known as a “stabilizer”. One of the most common dopants used to stabilise zirconia is yttrium oxide (Y_2O_3). This gives it a resistance to mode I cracking generally of the order of 5–8 $\text{MPa}\cdot\text{m}^{1/2}$ [11–13] and sometimes comparable to certain steels (potentially up to 16–17 $\text{MPa}\cdot\text{m}^{1/2}$ [14]). Another important property of yttriated zirconia is its accelerated ageing mechanism due to the action of water. Indeed, water in contact with the material infiltrated into microcracks progressively causes the tetragonal phase to change to the monoclinic phase [15]. Subsequently, there is an abnormal increase in the volume of meshes in contact with water, creating microcracks and propagating the phenomenon from near to near. This implies that any microcracking, whether present in the base material or after any potential shaping, will considerably degrade the service life of the final object. As a result, yttriated zirconia has very interesting characteristics for many fields. This material is the most common type of zirconia used in dentistry today and is increasingly considered the alternative to titanium for aesthetic dental implant abutments in final restorations, but also an alternative to stainless steels and titanium alloys for the luxury watchmaking industry, mainly to produce casing parts. However, because of its weaknesses, notably, the propagation of micro-cracks due to infiltration of aqueous solution, which reduces the service life of Y-TZP parts, analysis and reflection on the shaping stage, seem essential. In the dental sector, most denture prostheses are produced by milling or grinding. These operations generate high stresses, localised temperature increases and vibrations. The role of this stage in creating cracks or material tears must be minimised, as it has a direct impact on the life of the part produced.

Three main categories of materials are encountered when machining common ceramics: pre-sintered ceramics, sintered ceramics and glass-phase ceramics. The fundamental difference between these three groups is hardness. This implies a modification of the cutting parameters, the tools used and a different behaviour of the material when machined. In dentistry, glass-phase or sintered ceramics come in the form of calibrated blocks, potentially already fitted with a metal insertion screw at their base. These blocks

are conventionally machined directly at the dentist’s or prosthodontist’s workshop using diamond micro-grinders. Thus, it is possible to find studies discussing the surface finish obtained specifically for this type of application, but with higher values than those obtainable in finish micromachining [16] and the appearance of a monoclinic ceramic layer on the ground surface [17]. The major problems remain the fairly rapid degradation of tools by abrasive grain pull-out [18], marks left on machined surfaces and sharp edges and of course production time, which remains high due to low material throughput in the face of fairly large volumes to be removed from preformed blocks. Assistants are being investigated to speed up micro-rectification machining, in particular using a laser [19], but this does not appear to be conclusive for finishing operations due to crack propagation, despite increased tool life. Identical results are obtained when the workpiece is previously heated [20]. If the use of cutting tools is envisaged, diamond-coated carbide tools can give good surface finishes, even close to poly-mirror [21] but on a reduced surface as the tool life is very limited, likewise for cBN tools [13]. These approaches require inducing ductile cutting by material fragmentation rather than chip creation, which necessitates a negative local rake angle, very low feeds and great control over cutting conditions. This approach can be technically combined with the use of even higher-performance, but more fragile and more expensive, PCD natural or synthetic diamond tools, which are unsuitable for use by non-specialists in precision machining. All these limitations point end-users towards the machining of pre-sintered materials, for which it is nevertheless necessary to anticipate the volume shrinkage inherent in the final sintering phase. Very few studies have been published on the machining of ceramics in such a state [22]. However, some publications highlight, for example, the importance of the pre-sintering temperature before micro-milling [23] with the need to find a compromise between resistance to pull-out and crack propagation, and increased wear of the cutting tool used. Other studies on the machining of pre-sintered alumina with a high binder content (55% by volume) have highlighted the importance of the choice of tool and coating type for machining these highly abrasive materials even in the pre-sintered state, as well as for mitigating their high brittleness [6].

It is therefore essential to identify the various technical solutions for machining pre-sintered ceramics and to understand the phenomena occurring at the tool-material interface. Then, tool manufacturers could enhance their tool design for pre-sintered ceramics machining (substrate, coating but also geometry), and final users could choose the appropriate tooling and cutting conditions depending on the nature of ceramics they use, geometrical complexity and scale of the features to produce and production costs, time and surface quality they target. Some tool manufacturers

develop specific mills to machine dental ceramics (e.g. Franken dental, Datron, OSG Dental Industry) and leaders in the field of micro-milling solutions propose also some micro-mills specially designed for very abrasive materials (e.g. NS Tool, Hitashi Tools, Karnasch, Zecha, Magafor). This study was conducted with the support of the French manufacturer Magafor and in order to correspond to their knowhow and market, we selected a specific geometry and two types of coating proposed by the larger part of manufacturers for machining of pre-sintered ceramics, a PVD diamond-like coating and a CVD diamond coating, and another PVD coating already tested with success in contact with brittle and abrasive materials [24], even in front of ceramics particles [25] and third body presence [26]: AlCrN coating.

Most of the published works aim to bring out the influence of cutting conditions, grain size of the machined material, type of mill coating and tool integrity after a short machining length. Cutting tools are often coated with diamond or DLC, or sometimes, they present no coating at all. For example, Demarbaix et al. proposed to use the tool-material coupling standard NF E 66–520-5 in order to determine the optimal working range of a 3-mm ball-end mill with 2 flutes in pre-sintered Y-TZP [27]. They provide very useful reference cutting conditions, like a lowest limit of the cutting speed of 133 m/min with an axial depth of cut of 0.7 mm. After that limit, the tested slotting operations seem repeatable, and specific cutting energy remains relatively constant. It is underlined that the interaction between the tool and pre-sintered Y-TZP enables the transformation toughening mechanism. The range of adapted maximum chip thickness was identified between 0.035 and 0.070 mm. Then, a stable cutting regime can be obtained in ball-end milling of pre-sintered Y-TZP, but these reference values of speed, depth of cut and feed correspond to a macro-machining case and cannot be reached in micro-milling. Cutting conditions adapted to tool diameters equal or inferior to 1 mm have to be investigated in order to propose a suitable strategy for finishing complex micro-parts or micro-details as commonly encountered in dental or luxury applications. Chu et al. provide an experimental study that gives elements concerning the behaviour of different coatings after long machining lengths [28]. They reveal that the resistance to abrasion of the deposited coating has a huge influence on the tool life and that the ratio between grain size and surface roughness of the coating can play a representative role in wear mechanisms. Finding the appropriate coating is then a major issue in dental ball-end milling operations optimization. Irvine et al. focused on tool wear when ball-end milling of zirconia dental crowns [29] and showed that abrasion is clearly the main appearing wear mechanism and more precisely a third body abrasion which is really aggressive for the tool coating and substrate. It seems that diamond coatings are likely to have the resistance properties to withstand hard

particles third body abrasion and that the mean free path in tungsten carbide (average linear distance between WC grains) can be a sensitive parameter in this particular wear.

In the present study, original data is extracted from surface integrity, in-time force measurements and qualitative tool wear analyses in ball-end milling of pre-sintered 5Y-TZP. The main industrial targeted field is dental prosthesis manufacturing. For the experiments, 1-mm-diameter ball-end mills coated with AlCrN, DLC and diamond are used. This paper is divided into three main parts. Firstly, the experimental setup and methodology are exposed, including tool-specific design. Secondly, the experimental data concerning cutting forces, surface roughness and tool wear is presented and discussed. Finally, the conclusion presents the advantages and drawbacks of each coating as well as some interesting experiments to realise in order to refine the obtained results.

2 Experimental methodology

2.1 Workpiece material

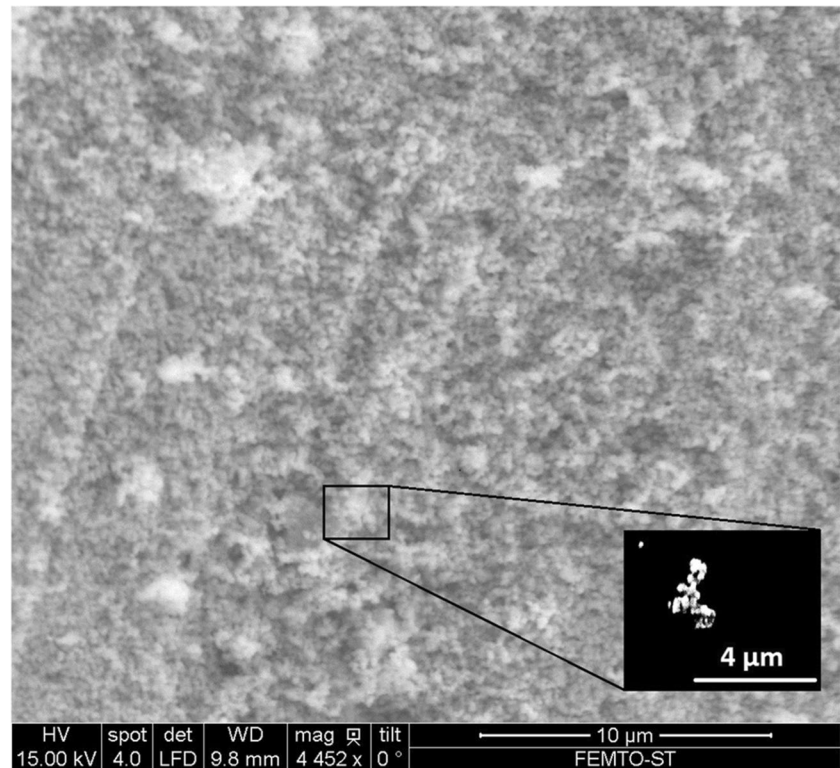
The machined material is a pre-sintered 5Y-TZP presenting a low hardness of 41 HV10 (± 1), a low Young modulus (11 GPa), no plastic domain and a high abrasiveness. The chemical composition is developed in Table 1. This material is commonly used in the dental industry to produce dental prosthesis. Its green state comes from a hot isostatic pressing at 800 °C as detailed in Shackelford et al. work, which permits a partial densification of the particles within the ceramic [30].

In this paper, all material and tool observations are performed with a FEI Quanta 450 W Scanning Electron Microscope. Figure 1 shows that the repartition of particle size is relatively uniform. It also allows us to observe the granular dimensions of the machined material ($< 0.300 \mu\text{m}$ in diameter). Moreover, the edge radius of micro-mills begins from a few micrometres ($\approx 1\text{--}8 \mu\text{m}$ in this paper). Therefore, the size effect due to the ratio between cutting edge radius and machined material grains, described by Bissacco et al. [31], would probably not affect significantly the cutting forces, but the material flow and tool wear would be very different than in the case of metal cutting and have to be discussed considering this specific microstructure.

Table 1 Chemical composition of the selected 5Y-TZP green ceramic (manufacturer's data)

Elements	Zirconium oxide ($\text{ZrO}_2 + \text{HfO}_2$)	Yttrium oxide (Y_2O_3)	Aluminium oxide (Al_2O_3)
Quantity (%mol)	94%	5%	< 0.4%

Fig. 1 Micrograph of the selected pre-sintered 5Y-TZP



2.2 Tools

A classical type of pre-finishing/finishing tool, adapted to the targeted field, is chosen: a 1-mm-diameter micro-grain tungsten carbide ball-end mill with two flutes. This is a fact that in the dental domain, it is uncommon to use tool diameters inferior to 1 mm because of the contouring approach when defining tool trajectories. Additionally, the relative geometrical roundness of a tooth implies that there is basically no necessity for a radius inferior to 0.5 mm to produce it. Moreover, it permits to avoid some scale effects well known in micro-milling, such as excessive deflexion, too limited cutting speed and chip thickness for example.

Parameters defining the global geometry of a micro ball-end mill are presented in Fig. 2. Local and global geometrical parameters of the selected tool are detailed in Table 2. All these characteristics were fixed after studying six references from the following providers: Datron, NS Tool, Karnasch, Zecha and Magafor (our partner here, with two different references). These reference tools present a similar design. The following information describes the main observed tendencies and how geometrical parameters were selected for the mill of test:

- All are micro-grain tungsten carbide hemispherical micro cutters with constant pitch and a head diameter D_0 of 1 mm, as they are selected to machine complex

surfaces of a few square millimetres with a good cutting accuracy and a good stiffness.

- These two teeth mills are the most common type of micro-cutters on the market, and they meet the technical limitations that these companies face in the production of the majority of their micro-tools.
- The edge radius r_β is small, about 2 or 3 μm before coating; the coating thickness has to be added to evaluate the final edge radius of each mill before machining.
- The orthogonal rake angle γ_0 is low, 0 or 5°, in order to keep a tough cutting edge but also to find an equilibrium between provoking a fracture of brittle materials instead of a regular shearing, and evacuating the cut material in the tool's grooves.
- The flank face is composed of two clearance zones, characterised by two different orthogonal clearance angles, between 12 and 20° for the primary angle $\alpha_{0,1}$, and between 23 and 40° for the secondary angle $\alpha_{0,2}$; the lateral clearance angle α_0 in the cylindrical part of the cutter is between 2 and 8°.
- The cutting length L_c along their axis varies from 0.75 to 4 mm, and we choose a medium value here in order to ensure a good evacuation of particles inside the grooves if the tool is confined in the material, as it can occur when contouring an entire tooth in a ceramic plate, but also a suitable tool stiffness.

Fig. 2 Main geometrical parameters of a micro ball end-mill

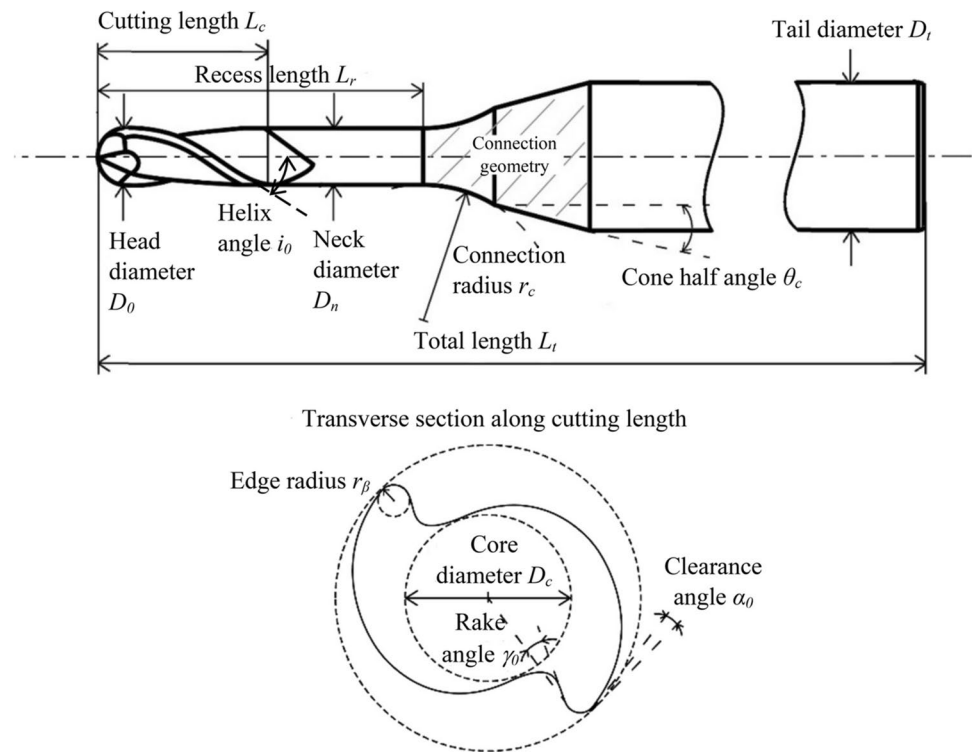


Table 2 Selected micro ball end-mill geometry

Head diameter D_0 (mm, 0/−0.012)	1
Number of flutes	2
Edge radius r_β before coating (μm , +/−1)	3
Orthogonal rake angle γ_0 (degrees, +/−1)	0
Primary clearance angle $\alpha_{0,1}$ (degrees, +/−1)	15
Secondary clearance angle $\alpha_{0,2}$ (degrees, +/−1)	30
Lateral clearance angle α_0 (degrees, +/−1)	2.5
Cutting length L_c (mm, 0/+0.1)	2.5
Helix angle i_0 (degrees, +/−1)	18
Core diameter D_c (mm, +/−0.05)	0.7
Recess length L_r (mm, 0/+0.5)	15
Neck diameter D_n (mm, −0.015/−0.035)	0.8
Connection radius R_c (mm, −0.04/−0.07)	2
Tail diameter D_t (mm, 0/−0.006)	4

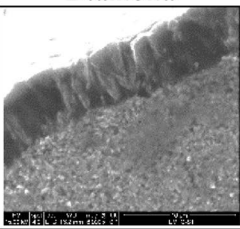
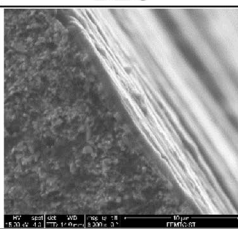
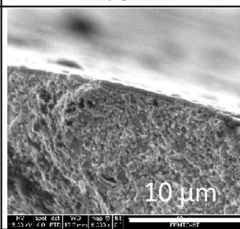
The helix angle i_0 is most of the time 30° , by tradition, but previous tests for micro-milling of hard steels [32] showed that an angle between 15 and 20° can be sufficient and permits to keep a more important core diameter to the tool.

- The core diameter D_c is huge compared to the head diameter on these mills; it goes from 0.6 to 0.7 because it should ensure a high stiffness of the tool and less deflexion when machining and then a higher loading before breakage.

- A quite huge recess length L_r of 15 or 16 mm is observed, in order to meet the specific characteristics imposed by the reduced volume of the machining environment when machining several teeth in a single ceramic plate; the neck diameter in this zone is between 0.8 and 0.95 mm.
- The connection between neck and tail sections is composed of a radius, a cone or a radius followed by a cone; the cone is really important in order to limit stress concentration in this zone during flexion; the radius R_c varies from 1 to 5 mm and the half cone angle θ_c from 12 to 21° ; the choice was fixed on a simple radius of 2 mm which seems to be sufficient in previous studies for machining of hard steels [32, 33] and in order to reduce settings and cost in the production of test mills.
- The tail of each cutter has a radius R_t equal to 3 or 4 mm, which seems to be a good compromise between the dynamic behaviour of the tool and clamping standard and limit torque in the tool holder.
- The total tool length L_t can be between 38 and 60 mm depending mainly on the length of the tool’s tail.

In dental prosthesis manufacturing, the range of products for tungsten carbide tools goes from uncoated until diamond-coated micro-mills. The most supplied coatings in the dental field have been chosen for this study: diamond coating obtained by CVD and DLC coating obtained by PVD (Table 3). AlCrN is usually proposed by tool providers to machine hard materials or as a less expensive alternative to diamond-based coatings in the

Table 3 Comparison between diamond, DLC and AlCrN coatings

Coating	Diamond	DLC	AlCrN
MEB observations of coatings thickness			
Coating thickness (μm)	5.5	0.7	0.4
Coating process	CVD	PVD-arc	PVD

face of abrasive materials. The diamond coating is the most usual one for green machining of Y-TZP. The two others are present in various domains. DLC is mostly used to machine aluminium alloy with or without lubricant as respectively shown in Sayuti et al. [34] and Fukui et al. works [35], whereas AlCrN rather serves for hardened steel milling, for example, in Escolle et al. [32] and Gilbin et al. works [33]. Moreover, as underlined in Section 1, some AlCrN coatings were also successfully tested in friction in the face of abrasive particles [24], even with ceramic particles and third body presence [25, 26]. Their thermal barrier efficiency and abrasion resistance distinguished these three tool coatings in front of the others. It has to be noted that for mills of diameter from 0.5 to 1 mm, DLC and AlCrN coatings lead to the same reference price about 40–50 €, but in the case of a diamond coating, the price of the mill can be multiplied easily by two.

Table 3 specifies coating thicknesses. These average values are estimated from a set of three SEM images taken along the cutting edge on a new tool after WEDM cutting and three more images taken after tool breakage because of unappropriated machining. They are consistent with the manufacturers' data. These values inform us in two different ways. Firstly, they give us an idea of the potential scale effect previously mentioned (the greater the coating thickness, the greater the cutting edge radius) which could influence the cutting process by modifying the cutting edge radius/chip thickness ratio. Secondly, they allow us to confirm if the coating is still present on the tool after machining. In dentistry, end users basically use general information to define cutting conditions, or these conditions are even already defined in the software solution without considering the type of tool which is used. That is why this study focuses on three coatings recommended by tool providers and attempts to clarify their operating range.

2.3 Machine tool and measuring device

As mentioned before, this study is focused on dental prosthesis manufacturing. Because of the performances of most currently used micro-milling machines, the spindle speed does not exceed 60,000 rpm or even 40,000 rpm most of the time. In this study, a Meyrat MHF-25 ER8/80 COD high-frequency spindle is used. It is able to rotate from 5000 to 80,000 rpm and was mounted on a Willemin-Macodel W418 5-axis milling centre.

The machining forces are measured using a high-sensitivity three-component dynamometer (Minidyn 9256C1) and a signal amplifier (5017B). Both are supplied by the Kistler company. This dynamometer was used in an adapted measuring range of –25 to 25 N and with a suitable sensitivity of 26 pC/N on the X and Z axes, and 13 pC/N in the Y direction (direction transverse to the feed in our configuration). Cross-talk between the three components is low, typically inferior to 2%. Natural frequency is high, superior to 5 kHz on each axis, which is three to five times more than teeth passing frequencies we tested, as recommended by the Kistler company if no acceleration compensation is used.

Surface topography at the bottom of the machined slots is digitised by using an Alicona Infinite Focus G4 confocal microscope. Linear and surface roughness criteria are calculated from recorded data by using *Digital Surf Mountains Map* software and by respecting all available ISO norms related to surface roughness measuring. Demarbaix et al. show a very stable surface roughness in macro ball-end milling of pre-sintered Y-TZP, with an average linear roughness of R_a around 0.08 μm [27]. From our experience, this criterion is not really discriminant in ball-end milling, particularly in considering micro-milling [32]. Hence, a surface criterion is used here for the analysis. It allows ruling out dispersions caused by the orientation of a linear surface measurement. This data is acquired on the surface using three patches of 500 × 300 μm with a resolution of 20 nm in

the X–Y plane and 10 nm on the Z axis. It allows us to have a better estimation of the surface criterion by averaging the results on these three successive patches.

2.4 Data processing

The evaluation criteria in this paper are machining forces, surface roughness and SEM observation of tool wear. The last one is only based on qualitative observations whereas the two others are quantitative.

The measured force signals allow us to distinguish maximum and minimum machining forces. They are obtained by averaging the local maxima and minima in order to plot two least squares constant functions (Fig. 3). This method permits to circumvent the problem of chaotic local signals, essentially due to the brittle nature of the used workpiece material. We consider that force amplitude tends to give an image of dynamical forces because the force amplitude is directly linked with the extreme configurations of the tool during machining, which is due to its dynamic behaviour. Force average represents basically the static forces tending to be constant all along machining.

Concerning the surface analysis, this study relies on a S_q^* parameter. It is defined like 3D amplitude S_q parameter, as established in the ISO standard 25178, but by omitting the separation between second- and third-order defaults. This choice is justified by two main reasons:

- This study is comparative and the dental prosthesis-manufacturing field uses aesthetic criteria in order to validate or not their final products. The use of surface parameters is relatively new as said in Leach's work [36], but it allows us to take into account the waviness defaults,

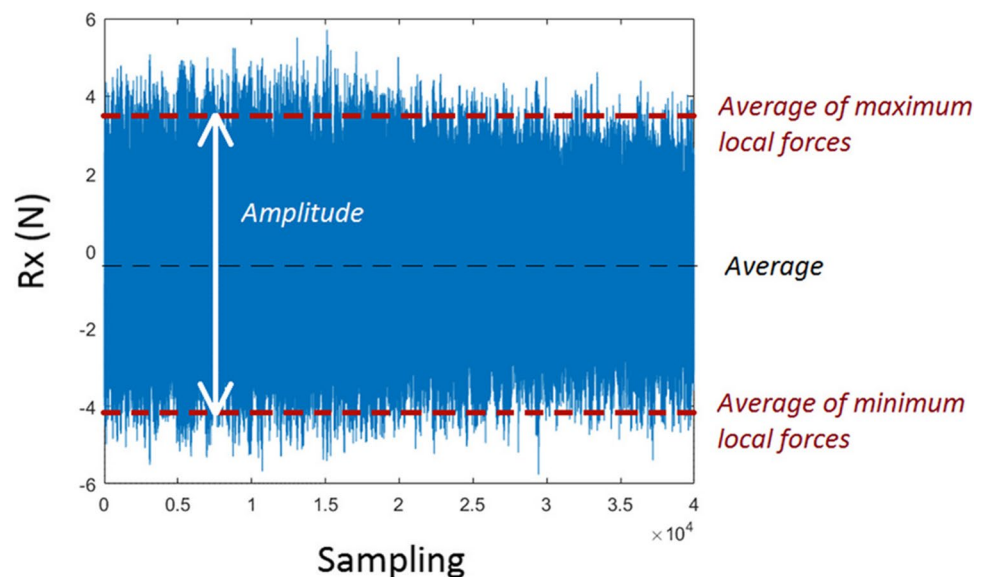
which are the most visually discernible, by keeping information about roughness.

- We have to consider that common linear parameters and filters used to separate roughness and waviness are defined from turning for a regular profile for the purpose of anticipating sealing or sliding issues. The associated standard gives no information concerning filter values that would be relevant to apply in milling for visual aspect or coating adherence purposes. Some works show that surface parameters allow us to reach a better value on correlation parameter R^2 compared to linear ones in this type of context. For example, in the case of a milled surface before NiP surface coating on a steel sample, when correlating the surface roughness to coating resistance in a pull-off adherence test, the correlation R^2 value starts from about 0.7 for linear criteria to 0.9 for surface criteria [37].

2.5 Design of experiments

The material sample is sawn from a dental wafer of 100 mm diameter and 16 mm thickness (supplied by Final Materials Company) by a step of 7 mm orthogonally to its circular basis. Samples are taken from the middle part of the wafer in order to limit the mass difference between each used samples. Pre-sintered 5Y-TZP being very brittle and having a low Young modulus, it is impossible to clamp directly the specimen. So each sample is stuck to an aluminium plate of $50 \times 39 \times 5 \text{ mm}^3$ with a strong glue. Then, this assembly is clamped on the upper side of the dynamometer (Fig. 4) using four screws M3 torqued to 1.5 Nm. Preliminary tests have proven, when machining a well-known 54 HRC steel [32, 33], that the film of glue and the intermediate aluminium plate do not disturb the data acquisition in this case.

Fig. 3 Plotting of the minimum, maximum, average and amplitude force functions in a given direction



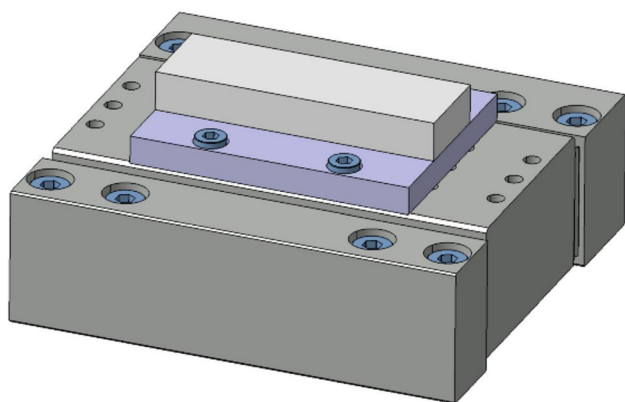


Fig. 4 3D representation of a sample clamped upon the Kistler dynamometer with an intermediate plate

To minimise planarity defects, a plan of $50 \times 16 \text{ mm}^2$ is previously milled on the upper face of the sample with a 6-mm-diameter NS-Tool square end mill in suitable machining conditions. This operation is performed after fixing the specimen on aluminium support in order to limit parallelism error between the aluminium support and the specimen. The same operation was previously performed on the aluminium support as well, ensuring a maximum error of parallelism of about 4 microns between the ceramic specimen and the dynamometer upper plate. This error was evaluated in situ by axial force detection with the dynamometer using the 1 mm mill itself, at ten different locations on the sample's surface.

Considering the abrasive properties of 5Y-TZP, its decline of mechanics performance in front of the water and the capacity of machining lubrication to reject micro-particles during milling [11], a vacuum cleaner is used (Kärcher DS 5800). It has two adapted air filters coupled with a water filtration and is set up aiming at a no-propagation of its vibrations to the machining area. It substitutes to particle evacuation role of lubrication by collecting a large part of the emitted powders during experimentation.

A simple machining operation is performed in this study: down-cutting shoulder milling with no tool/workpiece inclination and a radial depth of cut equal to half the diameter of the mill (Fig. 5). According to literature in green ceramics [27, 29] but also in metals [34, 35] and some preliminary tests performed in our laboratory, a down cutting mode is beneficial in terms of cutting forces and surface quality when using this type of mills at low feed for small diameters [32, 33]. A roughing operation is here targeted because of the extensive tool wear when machining this material, giving discriminating results. For this purpose, a half-radial immersion, common in roughing, is chosen. In the same way, no tool angle relative to the machine tool's vertical axis is considered here. This configuration tends to extend tool wear

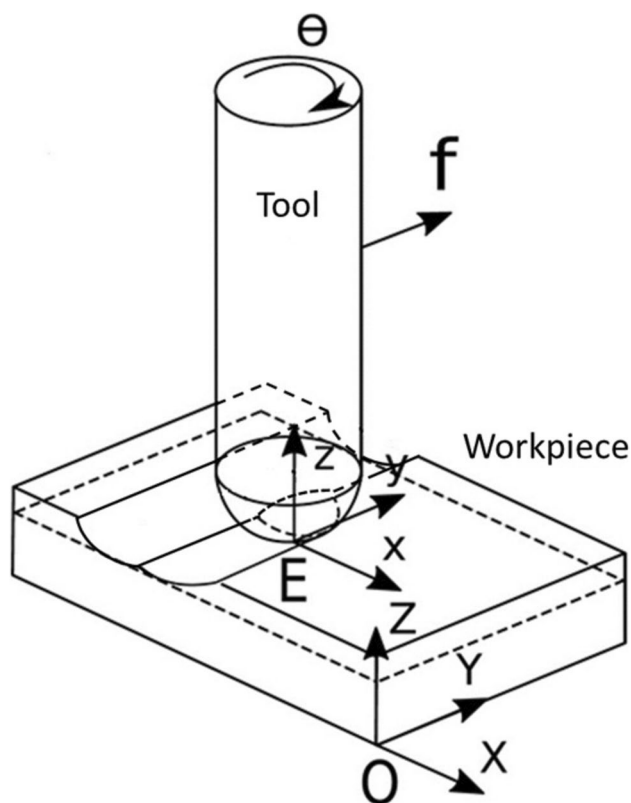


Fig. 5 Tested machining configuration

at tool tip and to limit the machined surface quality, but it appears to be the more common configuration in denture prosthesis or watch casing machining because of 2D contouring strategies that are used and sometimes because of the limitation of machines and CAM solutions final users could employ.

A spindle frequency of $N = 35,000 \text{ rpm}$ is taken according to industrial standard and corresponding to the higher stable zone identified for the test spindle with the help of acceleration measurement performed on the spindle nose at more than 100 different frequencies. The theoretical normal depth of cut d_n is fixed to an optimum of $150 \mu\text{m}$ according to preliminary tests. This value guarantees for the three tested mills the minimum growth of surface roughness and cutting forces for transverse inclinations from 0 to 80° in a down milling configuration along a machined length of 18 m . With no tool/workpiece inclination, d_n corresponds here to the axial depth of cut a_p . In this context, the most accurate way to measure the tool length and then ensure a limited but precise depth of cut is directly touching the workpiece until the dynamometer detects a contact force. The cutting speed V_c reaches a value of 78.5 m/min at the initial surface height in this configuration. The maximum value of these last trials—in flat machining with a feed per tooth (f_t) varying from 2 until $36 \mu\text{m/tooth}$ —permits to identify a common

stability zone in surface integrity for the three tested coatings at $f_t = 18 \mu\text{m}/\text{tooth}$. The surface roughness criterion S_q^* is then between 1 and $1.4 \mu\text{m}$ for the three tools with an advantage for DLC and diamond coatings. Concerning the evolution of cutting forces along a machined length of 18 m, the average resultant R_{xyz} stay between 1.5 and 2.3 N for AlCrN and DLC coatings and between 2.7 and 4.5 for diamond coating. In the same way, the average amplitude of R_{xyz} is between 2.5 and 3.8 N. The feed per tooth $f_t = 18 \mu\text{m}/\text{tooth}$ is then defined as a reference in this study. Finally, the length of machining (L_{max}) is set around 18 m in accordance

with common dental machining applications when roughing one tooth in a pre-sintered ceramic plate. These machining parameters are summed up in Table 4. All machining tests were repeated three times for each configuration.

3 Experimental results

3.1 Analysis of forces evolution compared to tool wear

Figures 6 and 7 are obtained through analysis of the force component R_{xyz} , which is the resultant of the forces on the X (R_x), Y (R_y) and Z (R_z) axes (square root of the sum of the square of each force component). In Fig. 6, the average value of R_{xyz} gives information about equivalent static loading which occurs in ball-end milling and would be responsible for compression and deflexion of the cutter. In Fig. 7, the pick-to-pick average amplitude of R_{xyz} informs about the performance of the cutter and its capacity to perform stable machining. Observed dispersions on R_{xyz} values (average and average amplitude) were always lesser than 10% when repeated three times each test, which ensures representative tendencies for Figs. 6

Table 4 Experimental machining parameters

Parameters	Values
Inclination from feed direction δ_f (°)	0
Inclination from a direction normal to the feed δ_n (°)	0
Spindle frequency N (rpm)	35,000
Normal depth of cut d_n (μm)—consistent to a_p here	150
Sweeping step (mm)—consistent to a_e here	0.5
Cutting speed along cutting edge V_c (m/min)	0 to 78.5
Feed per tooth f_t (mm/tooth)	0.018
Maximum machined length L_{max} (mm)	17,760

Fig. 6 Force average of the resultant R_{xyz} applied on the tool for the coating wear tests with $N = 35,000$ rpm, $d_n = 150 \mu\text{m}$, $\delta_n = 0^\circ$, $d_e = 500 \mu\text{m}$ and $f_t = 18 \mu\text{m}/\text{tooth}$

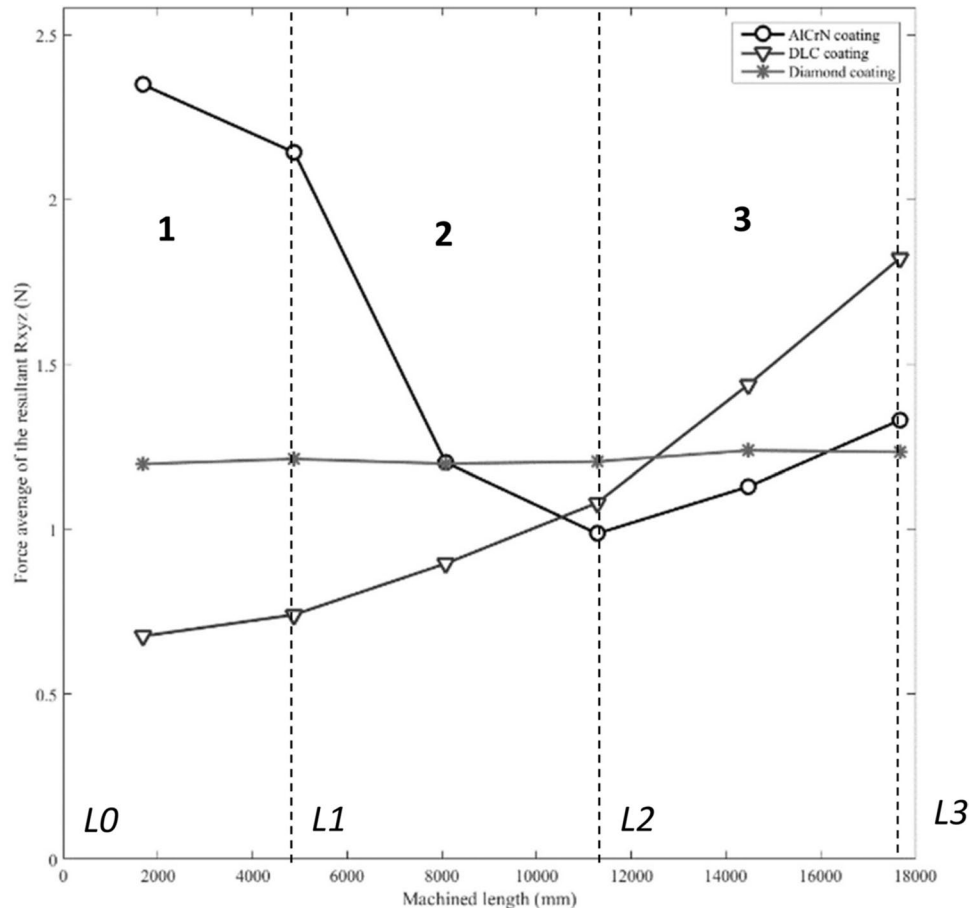
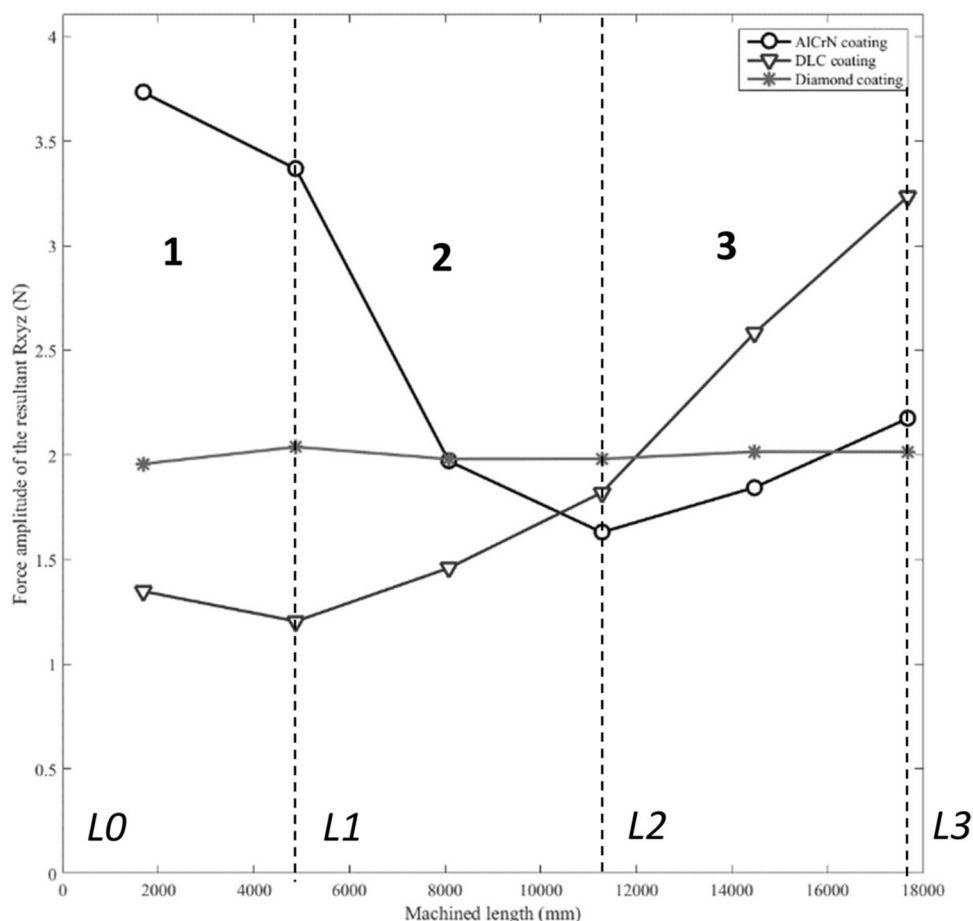


Fig. 7 Force amplitude of the resultant R_{xyz} applied on the tool for the coating wear tests with $N=35,000$ rpm, $d_n=150\ \mu\text{m}$, $\delta_n=0^\circ$, $d_e=500\ \mu\text{m}$ and $f_t=18\ \mu\text{m/tooth}$



and 7. Then, these representations of static and dynamic phenomena present similar variations for AlCrN and DLC coatings, when diamond coated tool shows no real variation along the tested machined length. This similarity between the two curves indicates that machining is stable and that it corresponds to the signature of a specific evolution in tool/workpiece interaction. These variations can be decomposed into three zones, named phases 1, 2 and 3. These high variations of forces for these two coatings indicate a high modification of the local tool geometry, while diamond coating does not present any visible variation even after 17,760 mm of milling. It would be interesting to observe the local geometry differences of each coating for the machining lengths that delimitate each phase. To analyse these zones, the following reference machined lengths are defined:

- $L0=0$ mm
- $L1=4,960$ mm
- $L2=11,360$ mm
- $L3=17,760$ mm

First, the AlCrN coating having the highest force variations between the three phases is studied. The tool-tip wear of this coating is presented in Fig. 8. All tools were cleaned with multidirectional airflow at 8 bars and 125 L/min for 10 s before observation with a microscope. At the end of phase 1, the coating on the cutting edge and the area near the flank faces is partially worn. Grooves appear on the machining area of the tool. At the end of phase 2, these grooves extend to a larger zone. Coating tearing observed at the end of phase 1 helps abrasion to grow as a third body finds a way to pass along the clearance surface, creating grooves of abrasion, as observed at the end of phase 2 (Fig. 9). At the end of phase 3, this abraded area is more extended than at the end of phase 2. The coating begins to disappear and the carbide is visible until the second flank face.

Besides, more specific observations of the cutting edge give interesting results for $L0$, $L1$, $L2$ and $L3$ (Fig. 10). Phase 1 contributes to sharpening the cutting edge of the new tool by ironing out coating defects due to PVD limitations for AlCrN coating. This sharpening continues until the end of phase 2. All these gathered observations permit us to deduce the machining behaviour for these two phases.

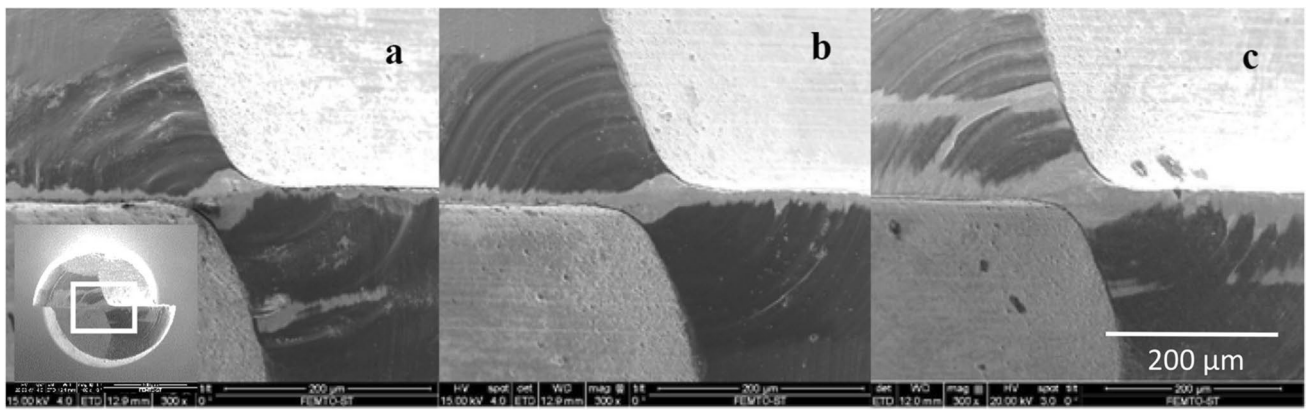


Fig. 8 Tip of the AlCrN-coated tool for machining lengths of $L1 = 4,960$ mm (a), $L2 = 11,360$ mm (b) and $L3 = 17,760$ mm (c)

Fig. 9 Evolution of the grooves because of abrasion on the tool tip for $L1 = 4960$ mm (left) and $L2 = 11,360$ mm (right)

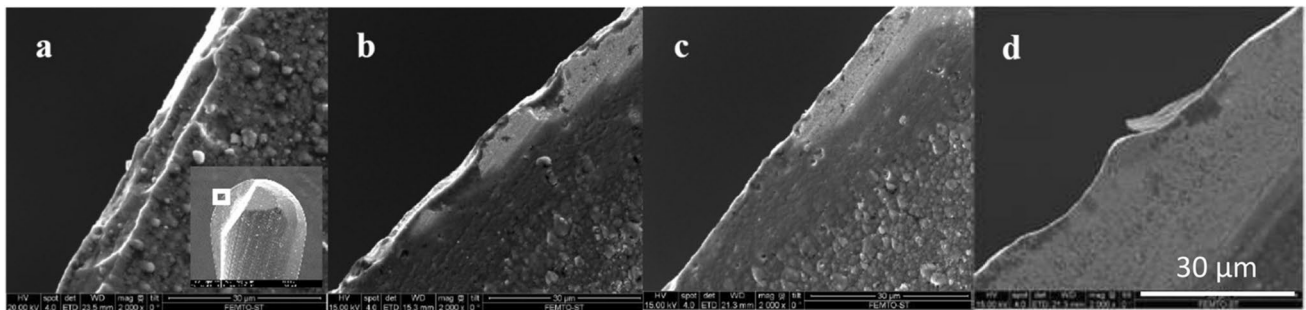
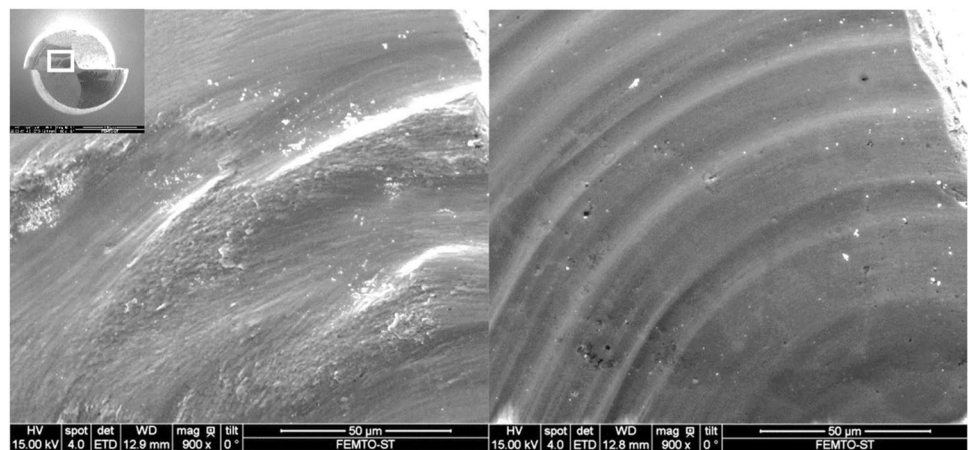


Fig. 10 Cutting edge on the border of the depth of cut $d_n = 150$ μm for $L0$ (a), $L1 = 4960$ mm (b), $L2 = 11,360$ mm (c) et $L3 = 17,760$ mm (d)

In phase 1, machining forces are relatively high because the new tool cutting edge does not promote the cutting of 5Y-TZP. Coating tearing on the flank faces creates grooves due to abrasion. These grooves do not promote material flowing on the tool tip during machining because of the chaotic geometry of these grooves.

At the beginning of phase 2, the cutting edge is relatively more sharpened than for $L0$. Cutting is promoted, and machining forces highly decrease until the end of this phase.

Another phenomenon is observable during phase 2. Indeed, an important decrease of the forces in the Z direction is visible during phases 1 and 2 by studying the average value of Rz force (Fig. 11). Forces transmitted to the workpiece—due to the pressure applied by the tool tip on the material—are relatively low. Besides, grooves appear on the tool tip during phases 1 and 2. It permits to have an increasing 5Y-TZP particle flow on the flank faces. The presence of a third body, which is described in Fillot et al. work [38], between the tool

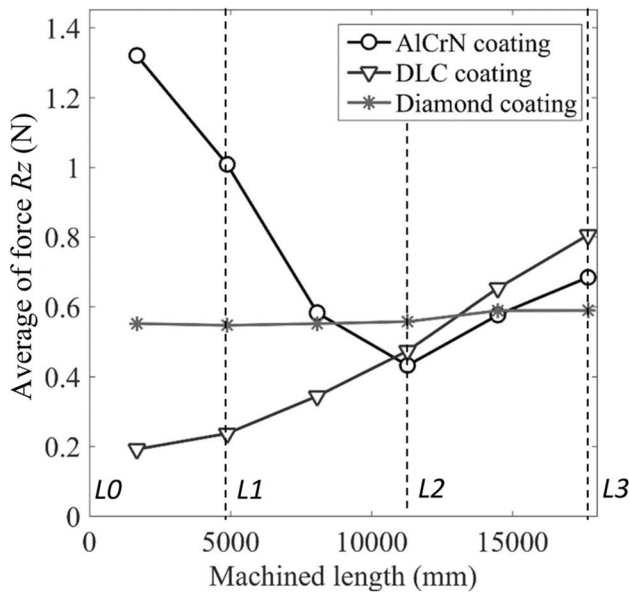


Fig. 11 Average of force R_z applied on the tool for the coating wear tests with $N=35,000$ rpm, $d_n=150$ μm , $\delta_n=0^\circ$, $d_e=500$ μm and $f_t=18$ $\mu\text{m/tooth}$

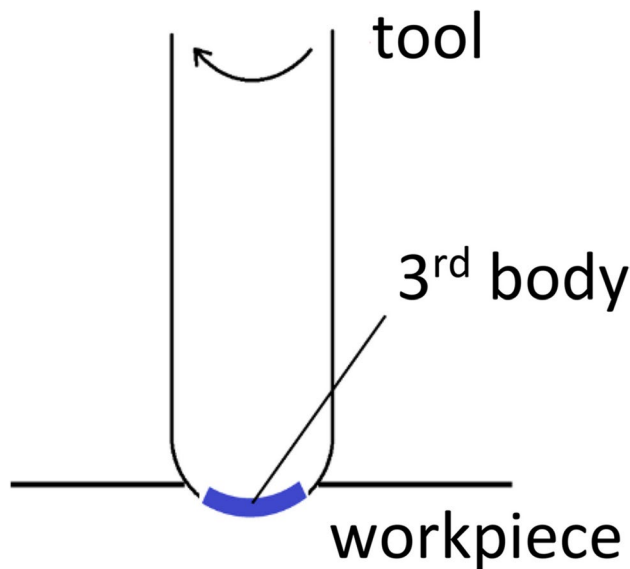


Fig. 12 Schematizing of the third body appearing

and the machined ceramic, partially explains this important and constant decrease of the force component R_z (Fig. 12). The drop of the resultant R_{xyz} is limited to phase 2. It can be explained by the combination between 5Y-TZP machining thanks to the third body and the cutting-edge sharpening, promoting cutting phenomena.

Wear may be defined as the way a contact loses its function. Here, it can be assimilated to a loss of mass by particles being detached from both materials in contact,

zirconia and coating or tungsten carbide. Thanks to a sampling of matter stuck on the tool after machining, we can observe that the third body is mainly composed of ceramic particles or small aggregates including less than 3% of particles coming from the tool (coating and tungsten carbide). These particles were abraded from the workpiece by the cutting process but also compression and friction between the cutting edge and clearance face of the tool and local machined surface. These two origins of particles gathered in the third body can be related to the source flow and the wear flow described by Fillot et al. [38]. According to these authors, the wear process constitutes a form of competition between the source flow and the wear flow. These two flows do not act directly on each other; rather they both modify the mass of the third body particles at the interface. They show that the main consequence of particle detachment is an increase in the mass of the third body. However, with the creation of an adequate interfacial layer (which supports the load and accommodates the difference in velocity), less particle detachment is expected. On the other hand, a particularly thick layer of the third body will probably give rise to the activation of the particle ejection process, while the ejection of particles themselves obviously decreases the mass of the third body. This ejection process seems to follow circular canals on the clearance face of the tool, right after the regular worn zone close to the cutting edge as shown in Fig. 8.

The reliability limits of the AlCrN-coated tool are reached in phase 3. It is due to the important lack of coating (Fig. 8) and a non-negligible deformation of the cutting edge compared to its initial geometry (Fig. 10). 5Y-TZP machining becomes chaotic. Machining behaviour with the third body does not predominate anymore in front of the high deformation of the cutting edge. At the beginning of this last phase, the tool is no longer usable because its machining behaviour is permanently degraded.

Machining force observations of the DLC-coated tool underline three classic phases (Figs. 6 and 7):

- Phase 1, honing
- Phase 2, progressive wear and milling in a non-degraded mode
- Phase 3, important increase of forces and wear acceleration

The wear of the tool tip for this coating with the same lengths previously evoked (L_0 , L_1 , L_2 and L_3) is visible in Fig. 13. With a lower machining length than the AlCrN coating, the border of the first and second flank faces is abraded. However, there is no groove appearing on the tool tip and wear is relatively homogeneous. DLC coating is almost absent on the first flank face at the end of phase 3. The tool carbide is uncoated in this area.

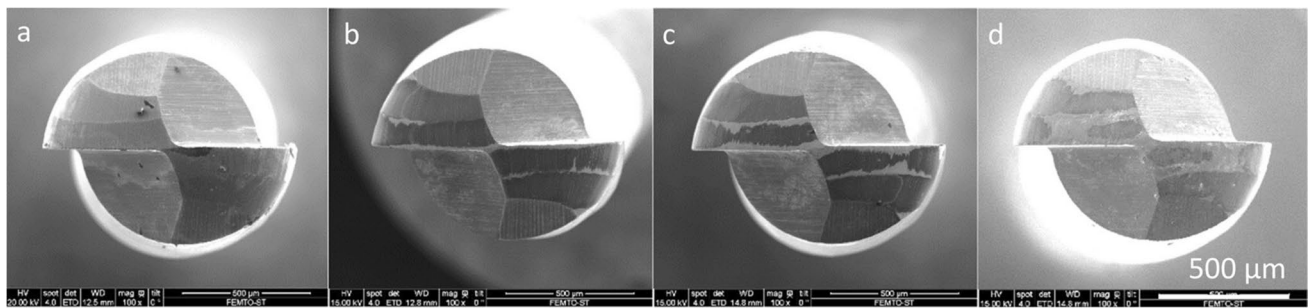


Fig. 13 Tool tip of DLC-coated tool for $L_0=0$ mm (a), $L_1=4960$ mm (b), $L_2=11,360$ mm (c) and $L_3=17,760$ mm (d)

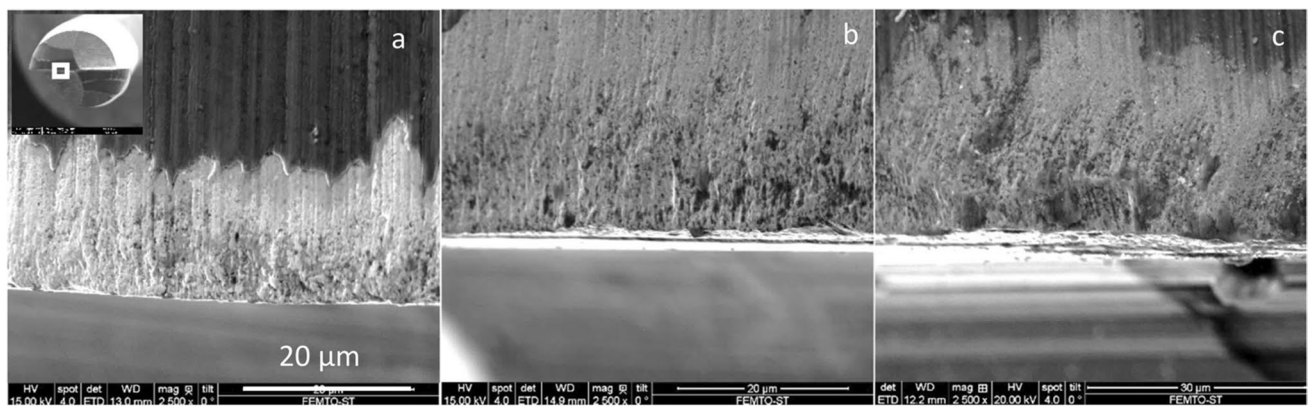


Fig. 14 Clearance face of cutting edge of the DLC-coated tool close to tool tip for $L_1=4960$ mm (a), $L_2=11,360$ mm (b) and $L_3=17,760$ mm (c)

A greater zoom level on the cutting edge of this tool permits to give an interpretation of average and amplitude variations of the R_{xyz} resultant (Fig. 14).

The coating disappears near the cutting edge on the first flank face at the end of phase 1. Nevertheless, there is no local geometry change on this cutting edge.

The first flank face begins to be dug in this same area after phase 2. The material machining is progressively degraded. It explains the increase of R_{xyz} gradients in phase 2 compared to phase 1.

At the end of phase 3, the cutting edge has serrations and a highly negative local cutting angle. It promotes a material ploughing that is more important than in phase 2. It explains the slight increase of R_{xyz} curve gradients in phase 3 compared to phase 2. The observed phenomena have unstable tendencies. This tool is considered unusable after a machining length of $L_2=11,360$ mm.

For the diamond coating, there is no visible variation in the amplitude and average of R_{xyz} . It could mean that there is no change in machining behaviour for $L_3=17,760$ mm, but it could also be a consequence of phenomena that compensate for each other. The diamond-coated tool is observed for L_1 , L_2 and L_3 to verify which hypothesis

is correct (Fig. 15). Abrasion impact on the cutting-edge geometry is visible but induced deformations are small. Indeed, the local cutting angle is the same between both machining lengths L_1 and L_3 . The coating is still on the tool after these wear tests contrary to DLC and AlCrN coatings. Thus, the R_{xyz} curve constancy is a consequence of the diamond coating roughness in front of 5Y-TZP machining. This coating is the best answer to dental prosthesis needs concerning tool life. It allows keeping the initial tool geometry after a machining corresponding to classical practices in this field.

To sum up the wear intensity of each coating, Fig. 16 shows the width of the band without coating on the flank face next to the cutting edge. These results are presented function of the machining length. Considering that the price of a DLC coating can be superior to a AlCrN one, the tool life of the mill with AlCrN coating could be more cost-effective. Concerning the tool with diamond coating, it seems that its cost, which could be easily two times higher, would be amortised if it is used with appropriate cutting conditions in precision machining of pre-sintered zirconia.

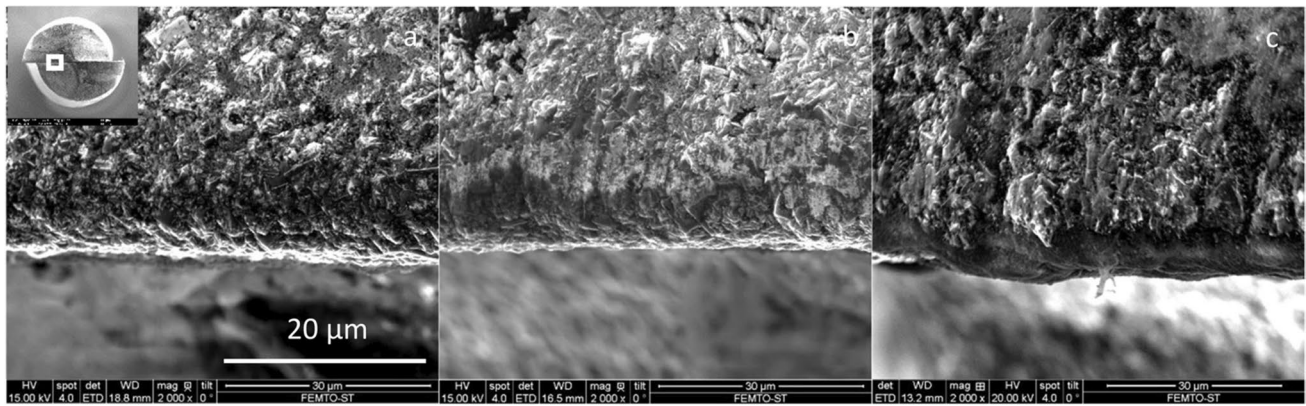
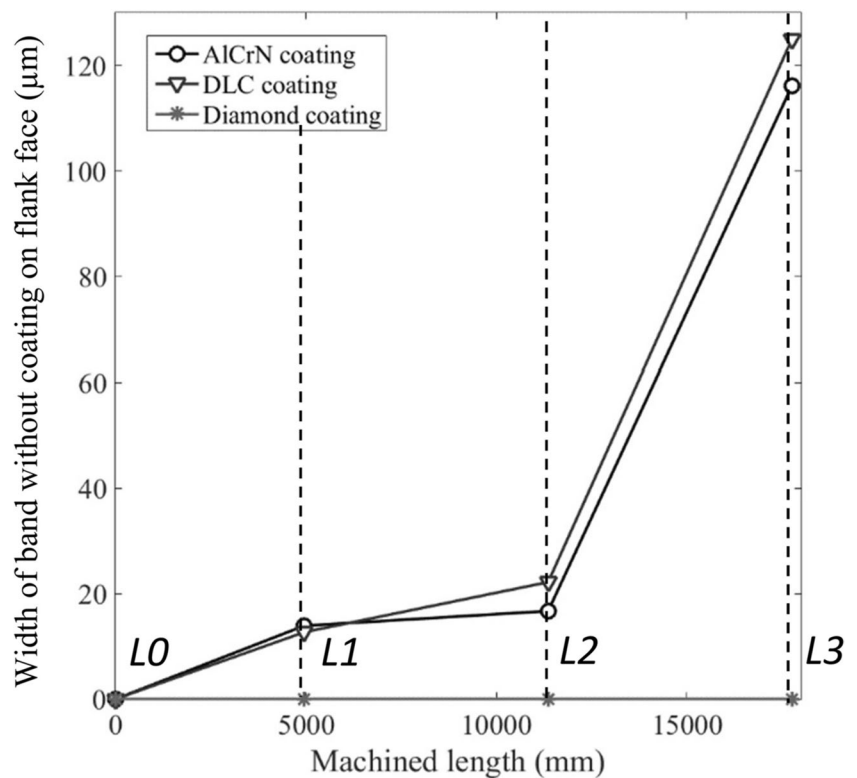


Fig. 15 Cutting edge of the diamond-coated tool from a top point of view for $L1 = 4960$ mm (a), $L2 = 11,360$ mm (b) and $L3 = 17,760$ mm (c)

Fig. 16 Width of coating wear on flank face



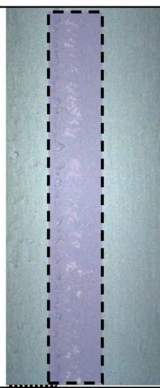
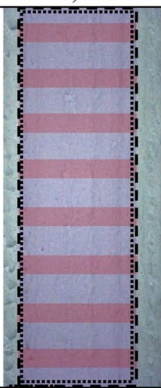
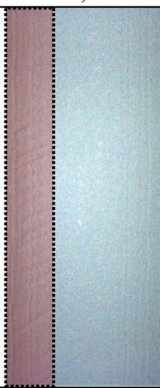
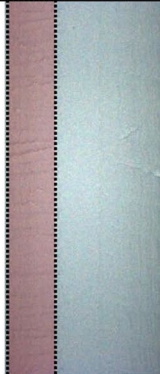
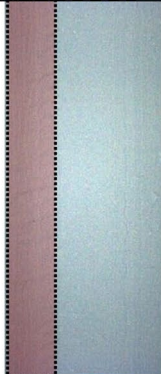

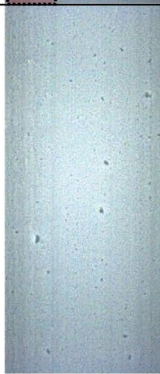

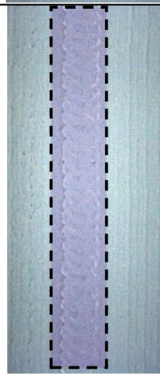


3.2 Surface integrity evolution

The surface obtained after certain lengths of milling also underlines several tendencies. In this field, 5Y-TZP behaviour does not seem like a metal relative to machining behaviour and non-intuitive results could appear when studying the surface integrity evolution.

Table 5 presents all the surface facies produced after milling for various coatings and machined lengths. For the AlCrN coating, the more the machining length rises, the more surface integrity improves. This phenomenon is explained by the progressive installation of the third

body. By the way, for this tool, the machined surface at the beginning is highly subjected to ploughing at the tool tip (as seen for a machined length of $L1 = 4.96$ mm for AlCrN in Table 5). Gradually, this ploughing effect widens at the centre of the slot until it disappears only letting the ingress of the teeth visible on the right side of the slot. This evolution confirms the third body wear mechanism. Indeed, next to the tool tip, there are no major changes in the local geometry between $L1 = 4.96$ mm and $L2 = 11.36$ mm while ploughing at the bottom of the slot almost disappears in this range of length. Therefore, machining is not carried out only by the tool geometry but by an intermediary that

Table 5 Overview of the different surface aspect depending on the machined length

Coatings	$L = 18 \text{ mm}$	$L = 4,96 \text{ mm}$	$L = 11,36 \text{ mm}$
AICrN			
DLC			
Diamond			
<p><i>Ploughing</i> </p> <p><i>Tearing</i> </p>			

grinds the material: a third body mainly constituted of the cut material.

Concerning the DLC coating, there are no important changes like the previous coating between $L0$ and $L2 = 11.36 \text{ mm}$. Nevertheless, it is important to underline three phenomena. Firstly, the propagation of cracks, noticeable for a machined surface with a new tool, has visually disappeared after $L1 = 4.96 \text{ mm}$. Secondly, the ploughing effect at the bottom of the slot, which is noticeable from the first tests, has increased a little (from $S_q^* = 1.05$ to $1.20 \mu\text{m}$). Finally, the ingress of the teeth is being promoted by the tool

wear after $L2 = 11.36 \text{ mm}$. It can be seen when looking at the chippings on the left side of the slot that progressively disappeared more as the machined length is high.

Concerning the diamond coating, there are two important observations to make. The first one concerns the ploughing at the centre of the slot. Indeed, this phenomenon appears gradually with the machined length. It is not observable in the resultant force variation of Rz because the force transmission from the tool to the ceramic is dumped in this direction. Thus, something is interposed between these two objects. Once again, taking into account remarks on

diamond and AlCrN-coated tools, the hypothesis of a third body wear seems to be one of the most suitable. Therefore, the ploughing could be an answer to a gradual filling of the coating porosities, which leads to ploughing phenomena at the bottom of the machined slot. This ploughing effect is not observed for the AlCrN coating because the prior dug grooves at the tool tip would permit a quick release of material particles during milling. In this case, there is not a sufficient pressure applied by the tool on the material to create a ploughing at the bottom of the slot. This ploughing effect may be avoided by setting a more effective particle aspiration or/and by a regular cleaning of the tool within the machine tool. The second phenomenon concerns the onset of little grooves on both sides of the machined surfaces. They are more numerous for greater machined lengths. It is explained by a progressive wear and chipping of the little coating grains on the mill surface, which let arise grains from the tool surface that are more massive. These massive grains pass along the clearance face of the worn tool; they machine the material during a non-negligible length because of the pre-sintered 5Y-TZP material nature. Figure 17 quantitatively sums up the surface integrity produced by each tool for selected reference lengths of machining.

4 Conclusions

This paper deals with an experimental investigation of three different coatings in a context of micro ball-end milling of pre-sintered 5Y-TZP for an unfavourable machining

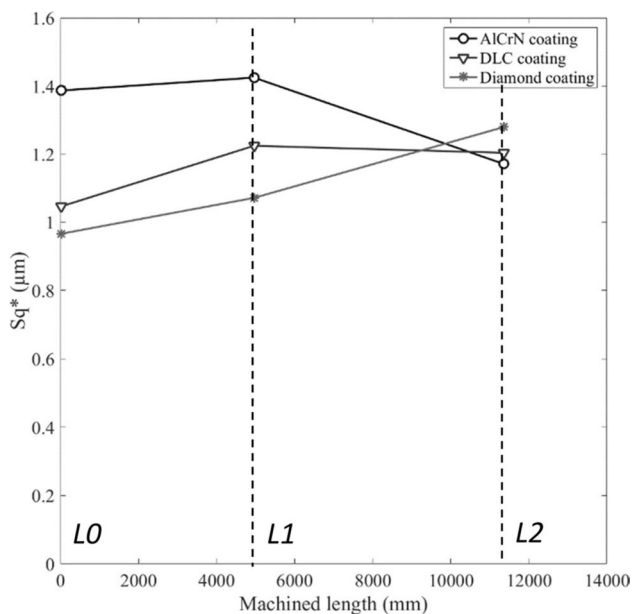


Fig. 17 Evolution of the S_q^* function of machined length for the three coatings

configuration common in industry: roughing milling with no tool/workpiece inclination in dry condition. The final purpose of this work was to enhance the geometry, coating and conditions of use of micro-ball-end mills applied in the dental industry. In this view, a reference geometry was determined from a study comparing the design proposed by different well-known providers. From this data, a specific design has been selected and produced by the Magafor company and then coated with a CVD diamond coating, a PVD diamond-like coating or a PVD AlCrN Coating. These tools presented two flutes, a rigid 4 mm tail diameter and 0.7 core diameter, a quite long recess length of 15 mm with 0.8 mm neck diameter, a 0° orthogonal rake angle and a $3 \mu\text{m}$ edge radius before the coating process. A preliminary experimental study conducted with the Magafor company showed that the following cutting conditions were suitable for the three reference tools in terms of cutting forces, stability and surface roughness: spindle frequency $N=35,000$ rpm ($0 \leq$ cutting velocity ≤ 78.5 m/min), normal depth of cut $d_n = 150 \mu\text{m}$, feed per tooth $f_t = 18 \mu\text{m/tooth}$. In this paper, experiments in roughing micro-milling with no tool/workpiece inclination and along a machining length of 18 m are presented. Monitoring of average and maximum values of cutting force resultant R_{xyz} , determination of surface roughness criterion S_q^* and SEM observations allowed us to analyse some phenomena and to underline the efficiency of each coating in these conditions:

- The AlCrN-coated tool wears relatively quickly. The behaviour of this tool varies a lot as forces data can underline it. However, the wear of this tool provokes a surface integrity stabilisation and even improvement. Nonetheless, it is highly detrimental to the mill. After 18 m of milling, the cutting-edge geometry highly changes due to a pronounced abrasion of the flank faces. It indicates that this amelioration, regarding the surface integrity, should probably achieve a critical point where the tool would have undergone too much wear to be still reliable.
- Concerning the DLC-coated tool, the wear is less pronounced than for the previous coating. The constant increase of cutting forces reflects an intensifying degradation of effective tool zones normally used to machine. Even if the surface integrity seems to be stabilised after $L1 = 4960$ mm of machining, thanks to local geometry changes induced by wear, the flank face is clearly affected by the machining process.
- The diamond-coated tool is the most resistant one during machining. Moreover, it presents a high cutting stability by studying all the forces components all along the wear tests. SEM observation confirms this because the wear of the mill stays anecdotal in front of both previous coatings. Nevertheless, this tool causes a degradation of

surface integrity after a certain length of machining. It involves worse results concerning this criterion at the centre of the machined slots in comparison with AlCrN and DLC coatings.

DLC and AlCrN coated mills showed both a change of behaviour after around 5 m of machined length, when their cutting edge starts to be worn and a third body takes place between the tool tip and the workpiece surface. From this moment, cutting forces and wear grew faster and grooves of abrasion appeared on the clearance face of these tools. DLC coating starts to disappear gradually when AlCrN coating presents some wear, then seems to be more resistant in the face of the third body until 11 m of machined length and then collapses quickly. All made observations indicate that the presence of a third body, mainly composed of abraded grains of zirconia, leads to the evolution of wear on tools' flank face, even if they present two successive and significant orthogonal clearance angles of 15 and 30°. Only the diamond tool seemed to be able to continue the machining in these conditions after 18 m of machined length and without notable wear.

Given this information, we can say that the choice of a suitable coating, even to machine pre-sintered material, is crucial to achieve an aimed surface integrity for short as for long time of use. It is clear that a CVD diamond coating is more efficient in protecting the micro-mill, but it generates a lesser surface quality in terms of surface roughness for important machining lengths. It is then suitable for roughing, and we can recommend using a new tool when starting the finishing process. Of course, this tool can be two or three times more expensive than the two others, and it is to consider too. AlCrN shows an interesting behaviour. It does not seem to be suitable for the targeted uses in the tested machining configuration, because of its relatively quick degradation. Nevertheless, if considering a more favourable tool-workpiece inclination, this coating could be suitable and more cost-effective than diamond tools, especially for finishing operations. The DLC coating is intermediary and constitutes a good compromise if only one tool is used to machine all the geometry, including finishing, but it is difficult to preconise this tool for a machining length of up to 20 m for the tested roughing machining configuration.

There are many prospects for this work. First of all, changes in local tool geometry (rake angle, first and second flank angle, flute depth) have to be tested in order to underline the potential influence of tool geometry on coating wear. In the same view, finishing tests could be performed with lower depths of cut and different tool/workpiece inclinations. It would be particularly interesting to see the behaviour of AlCrN coating in these conditions. The potential and limits of AlCrN coating are emphasised in this paper, but the use of multilayer AlCrN-based coatings would be very appropriate,

for example with a ceramic underlayer like TiSiN [39] or even a diamond one [40]. Other observation means, like high-speed camera or in situ wear measuring device, will allow going further in tool characterisation during machining. Moreover, the setting up of an automatic tool cleaning and the improvement of particle aspiration would be interesting to investigate in order to emphasise the effect of the first body constituted of ceramic particles. Moreover, as in the works of Kizaki et al., a pre-heating of the tool [19] or of the ceramic workpiece [20] can be tested in order to enhance the surface finish, or by the use of a laser impacting the surface just before milling, as in works of Kim and Lee [41]. But if the tool wear seems to be enhanced for the milling of sintered ceramics, it has to be validated in the case of pre-sintered 5Y-TZP. In addition, and to be relevant in dental manufacturing, parts obtained by 3D-printing methods such as DLP-stereolithography [42], have to be compared with machined parts in terms of quality, resistance in use time life but also in term of environmental impact. For applications needing a complex, unique and highly precise geometry, the printing-machining-sintering process chaining has to be investigated too.

Acknowledgements The authors thank sincerely Ing. Martial Personeni, Dr. Gérard Michel and Ing. Jean-Jacques Boy for their collaboration in setting up experiments and sample preparation. We would like to thank our industrial partner, the Magafor Company, for providing tools and funds to support the project in association with the French National Association for Technological Research (ANRT). This work used the micromachining and metrology facilities of the MIFHYSTO platform dedicated to the hybridization of micro-manufacturing techniques and the AMETISTE platform by the use of topomicroscopy. It was also partly supported by the French RENATECH network and its FEMTO-ST technological facility, MIMENTO, by the use of SEM. This work was carried out within the Manufacturing 21 network, which gathers about 20 French research laboratories. The covered topics are the study and modelling of the manufacturing processes, especially machining and additive manufacturing, and the emergence of new manufacturing methods.

Author contribution FM: conceptualization; methodology; investigation; visualisation; writing—original draft.

MF: conceptualization, methodology; supervision; funding acquisition; project administration; writing—review, editing and final draft.

AG: methodology; investigation; supervision; writing—review.

BE: methodology; investigation.

PP: supervision; funding acquisition; writing—review.

Declarations

Competing interests The authors declare no competing interests.

References

1. Masusawa T, Tönshoff HK (1997) Three-dimensional micromachining by machine tools. *Sci Tech Comm Pap* 8(2):621. [https://doi.org/10.1016/S0007-8506\(07\)60882-8](https://doi.org/10.1016/S0007-8506(07)60882-8)

2. Friedrich CR, Coane PJ, Vasile MJ (1997) Micromilling development and applications for microfabrication. *Microelectron Eng* 35:367–372. [https://doi.org/10.1016/S0167-9317\(96\)00198-0](https://doi.org/10.1016/S0167-9317(96)00198-0)
3. Keong Ng C, Melkote SN, Rahman M, Senthil Kumar A (2006) Experimental study of micro- and nano-scale cutting of aluminium 7075–T6. *Int J Mach Tools Manuf* 46:926–936. <https://doi.org/10.1016/j.ijmactools.2005.08.004>
4. Aramcharoen A, Mativenga PT (2009) Size effect and tool geometry in micromilling of tool steel. *Precis Eng* 33:402–407. <https://doi.org/10.1016/j.precisioneng.2008.11.002>
5. Câmara MA, Rubio JCC, Abrão AM, Davim JP (2012) State of the art on micromilling of materials, a review. *J Mater Sci Technol* 28(8):673–685. <https://www.jmst.org/EN/Y2012/V28/I8/673>
6. Mohanty S, Rameshbabu AP, Mandal S, Su B, Dhara S (2013) Critical issues in near net shape forming via green machining of ceramics: a case study of alumina dental crown. *J Asian Ceram Soc* 1(3):274–281. <https://doi.org/10.1016/j.jascer.2013.06.005>
7. Dadhich P, Srivas PK, Mohanty S, Dhara S (2015) Microfabrication of green ceramics: contact vs. non-contact machining. *J Eur Ceram Soc* 35(14):3909–3916. <https://doi.org/10.1016/j.jeurceramsoc.2015.06.025>
8. Ucuñ I, Aslantas K, Bedir F (2013) An experimental investigation of the effect of coating material on tool wear in micro milling of Inconel 718 super alloy. *Wear* 300(1–2):8–19. <https://doi.org/10.1016/j.wear.2013.01.103>
9. De Cristofaro S, Funaro N, Feriti GC, Comoglio M, Merlo A, Stefanini C, Dario P (2012) High-speed micro-milling: novel coatings for tool wear reduction. *Int J Mach Tools Manuf* 63:16–20. <https://doi.org/10.1016/j.ijmactools.2012.07.005>
10. Herráez-Galindo C, Rizo-Gorrita M, Maza-Solano S, Serrera-Figallo M-A, Torres-Lagares D (2022) A review on CAD/CAM yttria-stabilized tetragonal zirconia polycrystal (Y-TZP) and polymethyl methacrylate (PMMA) and their biological behavior. *Polymers* 14(5):906. <https://doi.org/10.3390/polym14050906>
11. Deville S, Chevalier J, Gremillard L (2006) Influence of surface finish and residual stresses on the ageing sensitivity of biomedical grade zirconia. *Biomaterials* 27(10):2186–2192. <https://doi.org/10.1016/j.biomaterials.2005.11.021>
12. Aragón-Duarte MC, Nevarez-Rascón A, Esparza-Ponce HE, Nevarez-Rascón MM, Talamantes RP, Ornelas C, Mendez-Nonell J, González-Hernández J, Yacamán MJ, Hurtado-Macias A (2017) Nanomechanical properties of zirconia- yttria and alumina zirconia- yttria biomedical ceramics, subjected to low temperature aging. *Ceram Int* 43(5):3931–3939. <https://doi.org/10.1016/j.ceramint.2016.12.033>
13. Romanus H, Ferraris E, Bouquet J, Reynaerts D, Lauwers B (2014) Micromilling of sintered ZrO₂ ceramic via cBN and diamond coated tools. *Procedia CIRP* 6th CIRP Int Conf High Perform Cut 14:371–76. <https://doi.org/10.1016/j.procir.2014.03.063>
14. Bravo-Leon A, Morikawa Y, Kawahara M, Mayo MJ (2002) Fracture toughness of nanocrystalline tetragonal zirconia with low yttria content. *Acta Mater* 50(18):4555–4562. [https://doi.org/10.1016/S1359-6454\(02\)00283-5](https://doi.org/10.1016/S1359-6454(02)00283-5)
15. Kobayashi K, Kuwajima H, Masaki T (1981) Phase change and mechanical properties of ZrO₂-Y₂O₃ solid electrolyte after ageing. *Solid State Ionics* 3–4:489–493. [https://doi.org/10.1016/0167-2738\(81\)90138-7](https://doi.org/10.1016/0167-2738(81)90138-7)
16. Song XF, Ren HT, Yin L (2016) Machinability of lithium disilicate glass ceramic in in vitro dental diamond bur adjusting process. *J Mech Behav Biomed Mater* 53:78–92. <https://doi.org/10.1016/j.jmbbm.2015.08.003>
17. Denkena B, Breidenstein B, Busemann S, Lehr C M (2017) Impact of hard machining on zirconia based ceramics for dental applications, *Procedia CIRP* 65:248–252. <http://creativecommons.org/licenses/by-nc-nd/4.0/>
18. Holthaus MG, Twardy S, Stolle J, Riemer O, Treccani L, Brinksmeier E, Rezwan K (2012) Micromachining of ceramic surfaces: hydroxyapatite and zirconia. *J Mater Process Technol* 212:614–624. <https://doi.org/10.1016/j.jmatprotec.2011.06.007>
19. Kizaki T, Harada K, Mitsuishi M (2014) Efficient and precise cutting of zirconia ceramics using heated cutting tool. *CIRP Ann Manuf Technol* 63:105–108. <https://doi.org/10.1016/j.cirp.2014.03.073>
20. Kizaki T, Sugita N, Mitsuishi M (2016) Experimental analysis of the machinability in the thermally assisted milling process of zirconia ceramics. *Precis Eng* 45:176–186. <https://doi.org/10.1016/j.precisioneng.2016.02.010>
21. Bian R, Ferraris E, He N, Reynaerts D (2014) Process investigation on meso-scale hard milling of ZrO₂ by diamond coated tools. *Precis Eng* 38(1):82–91. <https://doi.org/10.1016/j.precisioneng.2013.07.007>
22. Easler T, Khalfalla Y, Benyounis KY (2016) Green machining. Reference module in materials science and materials engineering. Elsevier. <https://doi.org/10.1016/B978-0-12-803581-8.03542-6>
23. Jian-Zhong L, Wu T, Yu ZY, Zhang L, Chen GQ, Guo DM (2012) Micro machining of pre-sintered ceramic green body. *J Mater Process Technol Micro-Manuf Process* 212(3):571–579. <https://doi.org/10.1016/j.jmatprotec.2011.10.030>
24. Mo JL, Zhu MH, Leyland A, Matthews A (2013) Impact wear and abrasion resistance of CrN, AlCrN and AlTiN PVD coatings. *Surf Coat Technol* 215:170–177. <https://doi.org/10.1016/j.surfcoat.2012.08.077>
25. Çay VV (2021) Effects of abrasive particle type, load and sliding distance on micro-abrasion resistance of high speed steel coated with AlCrN or AlTiN. *Mater Sci (Medziagotyra)* 27(1):1392–1320. <https://doi.org/10.5755/j02.ms.25776>
26. Birol Y, Isler D (2011) Abrasive wear performance of AlCrN-coated hot work tool steel at elevated temperatures under three-body regime. *Wear* 270(3–4):281–286. <https://doi.org/10.1016/j.wear.2010.10.069>
27. Demarbaix A, Rivière-Lorphèvre E, Ducobu F, Filippi E, Petit F, Preux N (2018) Behaviour of pre-sintered Y-TZP during machining operations: determination of recommended cutting parameters. *J Manuf Process* 32:85–92. <https://doi.org/10.1016/j.jmappro.2018.01.020>
28. Chu B, Zhu C, Samuel J, Kim GY (2013) Effect of grain-size on the micro-milling responses of aluminum-silicon carbide composites, 8th international conference on micromanufacturing ICOMM 2013 79:582–588
29. Irvine D, Goh WT, Dailami F, Matthews J (2019) The analysis of tool wear mechanisms in the machining of pre-sintered zirconia dental crowns. *Procedia Manuf* 38:1026–1033. <https://doi.org/10.1016/j.promfg.2020.01.188>
30. Shackelford JF, Doremus RH (2008) Ceramic and glass materials - structure, properties and processing. Springer. <https://doi.org/10.1007/978-0-387-73362-3>
31. Bissacco G, Hansen HN, De Chiffre L (2005) Micromilling of hardened tool steel for mould making applications. *J Mater Process Technol* 167:201–207. <https://doi.org/10.1016/j.jmatprotec.2005.05.029>
32. Escolle B, Fontaine M, Gilbin A, Thibaud S, Picart P (2015) Experimental investigation in micro ball-end milling of hardened steel. *J Mater Sci Eng A* 5(9–10):319–330. <https://doi.org/10.1007/s00170-017-1064-9>
33. Gilbin A, Fontaine M, Michel G, Thibaud S, Picart P (2013) Capability of tungsten carbide micro-mills to machine hardened tool steel. *Int J Precis Eng Manuf* 14(1):23–28. <https://doi.org/10.1007/s12541-013-0004-3>
34. Sayuti M, Tanaka T, Sarhan AAD, Saito Y, Hamdi M (2012) Surface quality improvement in CNC end milling machined aerospace AL-2017-T4 alloy using carbon onion nanolubrication with DLC

- cutting tool. Proceedings of the World Congress on Engineering, WCE 2012. Newswood limited, lecture notes in engineering and computer science 3:1487–1491
35. Fukui H, Okida J, Omori N, Moriguchi H, Tsuda K (2004) Cutting performance of DLC coated tools in dry machining aluminum alloys. *Surf Coat Technol* 187:70–76. <https://doi.org/10.1016/j.surfcoat.2004.01.014>
 36. Leach R (2013) Characterisation of areal surface texture. Springer Heidelberg New York Dordrecht London. <https://doi.org/10.1007/978-3-642-36458-7>
 37. Levrel E, Safie SN, Malécot P, Lambert V, Fontaine M, Hallez L, Lallemand S (2022) Functional correlation surface texture / grip of a deposit: case of NiP. *MATEC Web Conf* 368:01016. <https://doi.org/10.1051/mateconf/202236801016>
 38. Fillot N, Iordanoff I, Berthier Y (2007) Wear modeling and the third body concept. *Wear* 262(7):949–957. <https://doi.org/10.1016/j.wear.2006.10.011>
 39. Chen W, Yan A, Wang C, Deng Y, Chen DC, Xiao H, Zhang D, Meng X (2020) Microstructures and mechanical properties of AlCrN/TiSiN nanomultilayer coatings consisting of fcc single-phase solid solution. *Appl Surf Sci* 509:145303. <https://doi.org/10.1016/j.apsusc.2020.145303>
 40. Zhang J, Yuan Y (2020) Fabrication of AlCrN coatings on WC-Co substrates with diamond films interlayer. *Vacuum* 182:109715. <https://doi.org/10.1016/j.vacuum.2020.109715>
 41. Kim DH, Lee CM (2016) A study on the laser-assisted ball-end milling of difficult-to-cut materials using a new back-and-forth preheating method. *Int J Adv Manuf Technol* 85:1825–1834. <https://doi.org/10.1007/s00170-015-8014-1>
 42. He R, Liu W, Wu Z, An D, Huang M, Wu H, Jiang Q, Ji X, Wu S, Xie Z (2018) Fabrication of complex-shaped zirconia ceramic parts via a DLP-stereolithography-based 3D printing method. *Ceram Int* 44:3412–3416. <https://doi.org/10.1016/j.ceramint.2017.11.135>

Publisher's Note Springer Nature remains neutral with regard to jurisdictional claims in published maps and institutional affiliations.

Springer Nature or its licensor (e.g. a society or other partner) holds exclusive rights to this article under a publishing agreement with the author(s) or other rightsholder(s); author self-archiving of the accepted manuscript version of this article is solely governed by the terms of such publishing agreement and applicable law.